International Journal of Heat and Mass Transfer 52 (2009) 5371–5380

Contents lists available at ScienceDirect

International Journal of Heat and Mass Transfer

journal homepage: www.elsevier.com/locate/ijhmt

3D numerical simulation on shell-and-tube heat exchangers with middle-overlapped helical baffles and continuous baffles – Part I: Numerical model and results of whole heat exchanger with middle-overlapped helical baffles

Jian-Fei Zhang, Ya-Ling He, Wen-Quan Tao *

School of Energy and Power Engineering, Xi'an Jiaotong University, Xi'an 710049, China

ARTICLE INFO

Article history:
Received 17 March 2009
Received in revised form 9 July 2009
Accepted 9 July 2009
Available online 21 August 2009

Keywords:
Heat exchangers
Helical baffles
Numerical simulation
Turbulence
Pressure drop
Heat transfer

ABSTRACT

In the present study, a 3D numerical simulation of a whole heat exchanger with middle-overlapped helical baffles is carried out by using commercial codes of GAMBIT 2.3 and FLEUNT 6.3. At first, the computational model and numerical method of the whole heat exchanger with middle-overlapped helical baffles is presented in detail, and parallel computation mode is adopted for the simulation of a whole heat exchanger with six cycles of the middle-overlapped helical baffles of 40° helical angle on a grid system of 13.5-million cells; second, the validation of the computational model is performed by comparing the total pressure drop and average Nusselt number of the whole heat exchanger with experimental data. Reasonably good agreement is obtained, and the reasons causing to the discrepancy are analyzed. The shell-side fluid pressure and temperature fields of the whole area are then presented. Finally the cycle average Nusselt number of different cycle in the heat exchanger are compared and it is found that within the accuracy allowed in engineering computation, periodic model for one cycle can be used to investigate the heat transfer and pressure drop characteristics for different heat exchanger to save computational source. The companion paper will provide details of simulation results using the periodic model for different helical angles and different structures of helical baffles.

1. Introduction

Shell-and-tube heat exchangers (STHXs) are widely used in many industrial areas, such as power plant, chemical engineering, petroleum refining, food processing, etc. According to Master et al. [1] more than 35–40% of heat exchangers are of the shell-and-tube type due to their robust geometry construction, easy maintenance and possible upgrades. Baffle is an important shell-side component of STHXs. Besides supporting the tube bundles, the baffles form flow passage for the shell-side fluid in conjunction with the shell. The most commonly used baffle is the segmental baffle, which forces the shell-side fluid going through in a zigzag manner, hence improves the heat transfer with a large pressure drop penalty. This type of heat exchanger has been well-developed [2–5] and probably is still the most commonly used type of the shell-and-tube heat exchanger. The major drawbacks of the conventional shell-and-tube heat exchangers with segmental baffles (STHXsSB) are threefold: first it causes a large shell-side pressure drop; second it results in a dead zone in each compartment between two adjacent segmental baffles, leading to an increase of fouling resistance; third the dramatic zigzag flow pattern also causes high risk of vibration failure on tube bundle.

To overcome the above-mentioned drawbacks of the conventional segmental baffle, a number of improved structures were proposed for the purposes of higher heat transfer coefficient, low possibility of tube vibration, and reduced fouling factor with a mild increase in pumping power [5–10]. However, the principal shortcomings of the conventional segmental baffle still remain in the above-mentioned studies, even though the pressure drop across the heat exchangers has been reduced to some extent. A new type of baffle, called helical baffle, provides further improvement. This type of baffle was first proposed by Lutcha and Nemcansky [11], where they investigated the flow field patterns produced by such helical baffle geometry with different helix angles. They found that these flow patterns were much close to plug flow condition, which was expected to reduce shell-side pressure drop and to improve heat transfer performance. Stehlik et al. [12] compared heat transfer and pressure drop correction factors for a heat exchanger with an optimized segmental baffle based on the Bell–Delaware method [2–4] with those for a heat exchanger with helical baffles. Kral et al. [13] discussed the performance of heat exchangers with helical baffles (STHXsHB) based on test results of various baffles geometries. A comparison between the test data of shell-side heat transfer coefficient versus shell-side pressure drop was provided for five

* Corresponding author.
E-mail address: wqtao@mail.xjtu.edu.cn (W.-Q. Tao).

0017-9310/$ - see front matter © 2009 Elsevier Ltd. All rights reserved.
doi:10.1016/j.ijheatmasstransfer.2009.07.006

Nomenclature

Latin symbols

A_o	heat exchange area based on the outer diameter of tube, mm^2
B	baffle spacing for segmental baffles or helical pitch for helical baffles, mm
c_p	specific heat, J/(kg K)
D_i	inside diameter of shell, mm
D_o	outside diameter of shell, mm
D_1	tube bundle-circumscribed circle diameter, mm
d_i	tube inner diameter, mm
d_o	outer diameter of tube, mm
E_{ij}	mean rate-of-strain tensor
h	heat transfer coefficient, W (m^2 K)$^{-1}$
k	turbulent kinetic energy
l	effective length of tube, mm
M	mass flow rate, kg/s
N	tube number
N_t	number of tube rows
Nu	Nu number
Δp	shell-side pressure drop, kPa
q_s	volume flow rate, m^3 h^{-1}
Re	*Re* number
S	cross-flow area at the shell centerline, mm^2
Δt_m	logarithmic mean temperature difference, K
t	temperature, K
t_p	tube pitch, mm
u	fluid velocity in the shell side, m s^{-1}

Greek symbols

β	helix angle
ε	turbulent energy dissipation
Φ	heat exchange quantity, W
λ	thermal conductivity, W (m K) $^{-1}$
μ	dynamic viscosity of fluid, Pa s
ν	kinematic viscosity of fluid, m^2 s^{-1}
ρ	density of fluid, kg m^{-3}

Subscripts

in	inlet
out	outlet
s	shell side
t	tube side
w	wall

helical baffles and one segmental baffle measured from a water-water heat exchanger. The case of 40° helix angle behaved the best. For the convenience of manufacturing, up to now all helical baffles actually used in STHXs are noncontinuous approximate helicoids. The noncontinuous helical baffles are usually made by four elliptical sector-shaped plates joined end to end. Elliptical sector-shaped plates are arranged in a pseudohelical (noncontinuous) manner, as shown in Fig. 1, where the helix angle, designated by β, and helical pitch, B, are presented. As shown in Fig. 1 the helix angle is referred to the angle between normal line of circular sector-shaped plates and the axis of heat exchanger. Each baffle occupies one-quarter of the cross section of the heat exchanger and is angled to the axis of the heat exchanger. The two adjacent baffles may touch at the perimeter of each sector, forming a continuous helix at the outer periphery (Fig. 1); and this structure of connecting baffles together is called continuous connection. Another connection between two adjacent sectors is the middle-overlapped connection as shown in Fig. 2. For heat exchangers with large shell diameters, such structure can reduce the helical pitch to shorten the length of heat exchanger, and can also reduce the cross-flow area to obtain a higher shell-side velocity. Hence such connection is more popular in engineering practice. In this paper helical baffle refers to such noncontinuous baffle, otherwise special description will be given. Above papers were mostly published in the last century. Typical publications on this subject since the year of 2000 can be referred to [14–18]. Experimental study on heat transfer enhancement of a helically baffled heat exchanger combined with three-dimensional finned tubes was conducted by Zhang et al. [15]. Peng et al. [16] carried out an experimental study of shell-and-tube heat exchangers with continuous helical baffles and they found that that the use of continuous helical baffles resulted in nearly 10% increase in heat transfer coefficient compared to that of conventional segmental baffles based on the same shell-side pressure drop. Lei et al. [17] presented some experimental results of pressure drop and heat transfer of a heat exchanger with helical baffles. A comprehensive comparison of heat transfer coefficient per unit pressure drop and unit pumping power at the same shell-side flow rate was provided for four helical baffle heat exchangers and one segmental baffle heat exchanger by Zhang et al. [18].

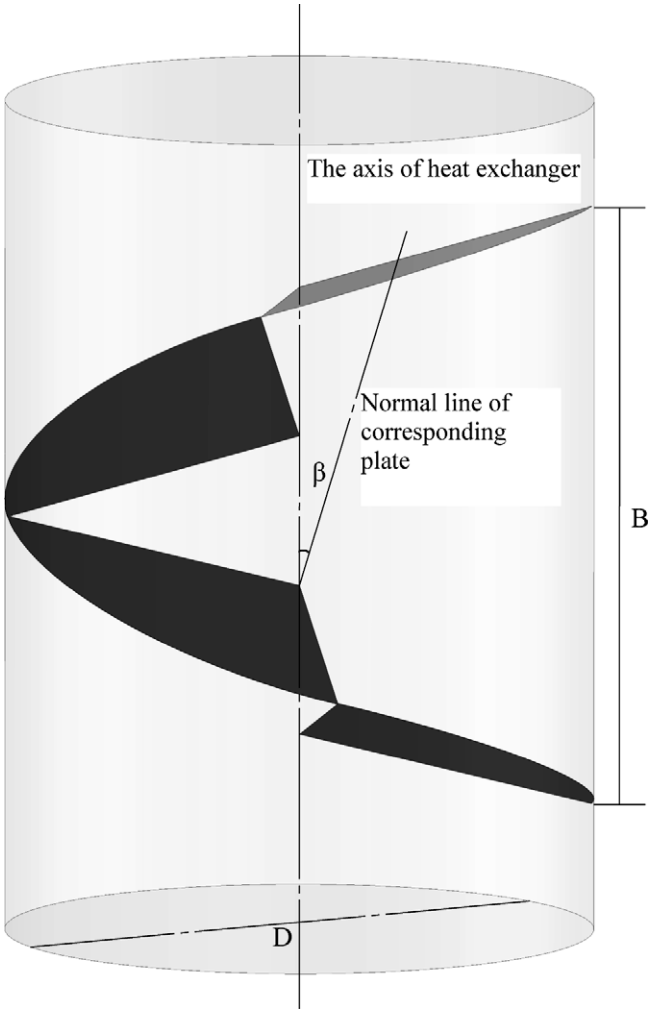

Fig. 1. Schematics of parameters definition.

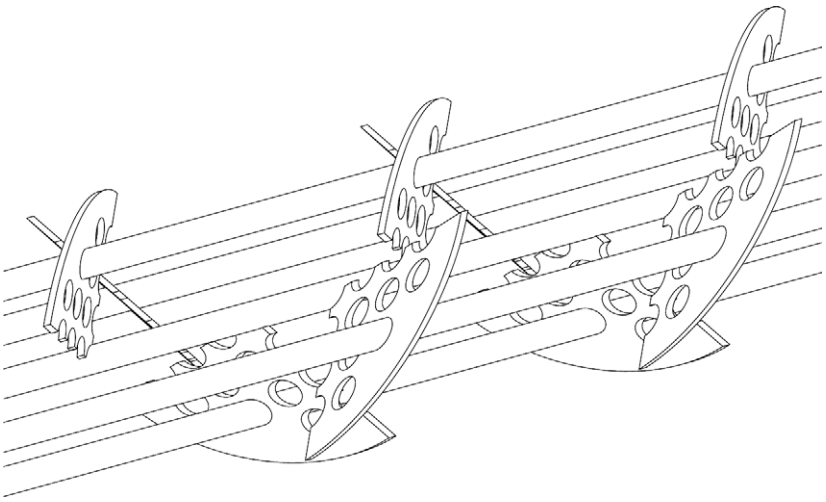

Fig. 2. Four pieces middle-overlapped helical baffle arrangement.

Another important research method for the improvement of heat exchangers is the numerical simulation. Although experiment study can provide reliable test data for designers and researchers, it is very expensive and time consuming. Compared to experiment, a validated CFD method can provide more information in heat exchangers at much lower cost. In the following a brief review on the numerical simulation study is presented. In 1974, Patankar and Spalding [19] simplified a three-dimensional STHX to a kind of porous media model and introduced the concept of distribution resistance to simulate the shell-side flow in STHX. In 1978, Butterworth [20] developed a three-dimensional model for heat transfer in tube bundles. From 1980 to 1982, porous media model and distribution resistance concept was improved by Sha [21] and Sha et al. [22], and the concept of surface permeabilities was introduced to account for the anisotropy of tube bundles porosities. Prithiviraj and Andrews [23–25] developed a three-dimensional CFD method (named as HEATX) based on the distributed resistance concept along with volumetric porosities and surface permeabilities to simulate flow and heat transfer in STHXsSB. Their research results were compared with experiment data and good agreement between the simulation results and experimental data was obtained. In 2003, Deng [26] investigated the flow and heat transfer in shell side of STHXsSB and flow in shell side of STHXsHB based on the method suggested by Prithiviraj and Andrews [23–25], and the accuracy of numerical model was validated by experimental data. In 2005, Andrews and Master [27,28] employed HEATX to investigate the performance of a STHXHB. Their computed pressure drops compared reasonably well with ABB Lummus Heat Transfer Co. pressure drop correlation results. The numerical model with porous medium concept mentioned above could reduce the requirement to computer capability greatly, but there are still some defaults in it: (1) many additional parameters, such as volumetric porosities and surface permeabilities on shell side of heat exchanger must be calculated exactly. Because the shell-side configuration of STHXs is very much complicated, so it is a big challenge for researchers and designers to obtain such geometric parameters accurately; (2) the shell-side distributed resistances and heat transfer coefficient must be provided from existing experimental correlation formulas, and the accuracy of numerical results is affected by such correlations to a great extent; (3) detailed and exact characteristics of flow and heat transfer on shell side cannot be obtained due to the simplified principle of porous media model. Among the three drawbacks, the second one is probably the most fatal.

Recently, the rapid development of CFD commercial code and computer hardware helps the direct 3D numerical simulation of complex flow phenomenon in STHXs and it is becoming more and more convenient and popular. Schröder and Gelbe [29] applied two- and three-dimensional simulation models for the computation of flow-induced vibration of tube bundles. Mohr and Gelbe [30] presented a method to produce equivalent velocity distributions and corresponding cross-sectional areas in tube bundles of STHXs, which enables the designer to predict the vibration excitation more accurately than before. Philpott and Deans [31] investigated the effects of the addition of ammonia on the enhancement of steam condensation heat transfer in a horizontal shell-and-tube condenser. Karlsson and Vamling [32] carried out 2D CFD calculations for vapor flow field and rate of condensation for a pure refrigerant and a binary mixture in a shell-and-tube condenser. Lee and Hur [33] investigated the heat transfer and flow in the shell side of a STHXSB, and the effects of locations and sizes of the sealing strips on heat transfer and flow were also investigated in their study. Apart from the numerical study on STHXsSB mentioned above, several numerical studies on STHXsHB were also conducted by some researchers. Shen et al. [34] established a mathematical model of the flow and heat transfer of the helical baffles heat exchanger to simulate the influence of helical baffles on heat transfer and flow characteristics of STHXsHB. And the numerical simulation results at the 35° helix inclination angle were compared with experimental data. Lei et al. [35] investigated the effects of helix angle on the flow and heat transfer characteristics of STHXs with continuous baffles by using simplified periodical model. Lei et al. [17] also designed a heat exchanger with two-layer helical baffles and compared its performance with heat exchanger with single-segment baffles and single-helical baffles by using simplified periodical numerical model. Jafari Nasr and Shafeghat [36] studied the velocity distribution in STHXsHB at different helix angles and developed a rapid algorithm for STHXsHB design.

In most of the above referenced papers for the performance simulation of STHXsHB a periodic model is usually adopted for which the fluid flow and heat transfer are assumed to be fully developed. For the external fluid flow and heat transfer it is well accepted [37–39] that for the flow and heat transfer in a geometric periodic structure it needs about 4–6 cycles for the flow and heat transfer to be fully developed. For many STHXsHB in practical usage, the cycle numbers are not very far from above-mentioned lower limitation. Thus only periodical model is not enough to understand the full fluid flow and heat transfer process in the STHXsHB. At least we have to reveal how many cycles (the space

within one helical pitch composes one cycle) are needed in a STHXHB for the shell-side flow and heat transfer to be fully developed. In addition, as indicated above the STHXsHB in practical application are all of noncontinuous type, and the experimental comparative study between continuous and noncontinuous baffles has not been reported in the literatures, probably because the expensive test cost. Thus numerical comparison will be very useful to proceed such an investigation.

In the present paper, a 3D simulation model on flow and heat transfer in the shell side of a whole STHXHB with middle-overlapped baffles at 40° helix angle will be established in detail by using the commercial software of FLUENT with grid systems being generated by GAMBIT. Numerical simulation for the whole heat exchanger with 40° helix angle will first be conducted at a series of shell-side flow rate for validating the numerical model. The simulated results will be compared with some experiment data available to the present authors. Then numerical results of the whole heat exchanger simulation will be presented in details, including the streamwise variation of the cycle average Nusselt number, the shell-side fluid pressure drop and temperature distributions. It will be shown that after 5 or 6 cycles the flow and heat transfer in a STHXHB can be regarded as fully developed, validating the significance of periodic model in the numerical simulation of STHXsHB. In the companion paper the periodic model will be adopted for the simulation. Investigation will be conducted for three periodic models with middle-overlapped baffles at different helix angles to reveal the fully developed performance, and the effects of helix angle on the performance of STHXsHB are examined and analyzed by the field synergy principle recently developed by Guo et al. [40–42] and later enhanced in [43–49]. The performance of a periodic model with continuous helical baffle will also be established and simulations will be conducted. The numerical results will be analyzed from different aspects: the effects of the helix angle, comparison between the results of continuous helical baffle with noncontinuous middle-overlapped helical baffles for the shell-side heat transfer and pressure drop at the same flow rate, and the comparison between the two types of helical baffles for the shell-side heat transfer coefficient based on the unit pressure drop.

2. Model for whole heat exchanger simulation

2.1. Computational model

The computational model of an experimental tested STHXHB with 40° helix angle [18] is shown in Fig. 3, and the geometry parameters are listed in Table 1. As can be seen from Fig. 3, the simulated STHXHB has six cycles of baffles in the shell-side direction with total tube number of 37. The whole computational domain is bounded by the inner side of the shell and every thing in the shell is contained in the domain. The inlet and outlet of the domain are connected with the corresponding tubes.

To simplify numerical simulation while still keep the basic characteristics of the process, following assumptions are made: (1) the shell-side fluid is of constant thermal properties; (2) the fluid flow and heat transfer processes are turbulent and in steady-state; (3) the leak flows between tube and baffle and that between baffle and the shell are neglected; (4) the natural convection induced by the fluid density variation is neglected; (5) the tube wall temperatures are kept constant in the whole shell side; (6) the heat exchanger is well-insulated hence the heat loss to the environment is totally neglected.

2.2. Governing equations and boundary conditions

The renormalization group (RNG) k–ε model [50–52] is adopted because it can provide improved predictions of near-wall flows and flows with high streamline curvature [50,51]. The governing equations for the mass, momentum, and energy conservations, and for k and ε can be expressed as follows:

Mass:

$$\frac{\partial}{\partial x_i}(\rho u_i) = 0 \tag{1}$$

Momentum:

$$\frac{\partial}{\partial x_i}(\rho u_i u_k) = \frac{\partial}{\partial x_i}\left(\mu \frac{\partial u_k}{\partial x_i}\right) - \frac{\partial p}{\partial x_k} \tag{2}$$

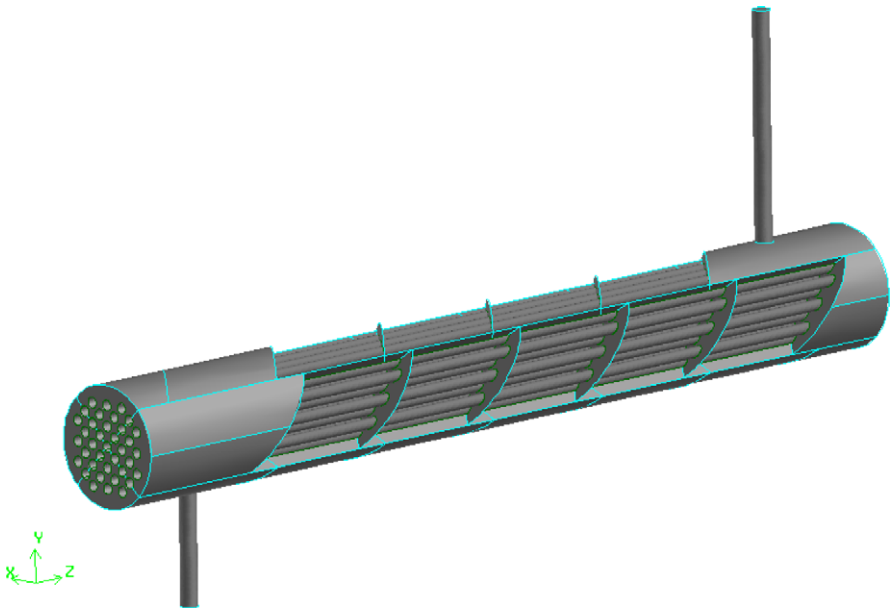

Fig. 3. Shaded partial scenograph of the computational model.

Table 1
Geometry parameters for the whole model.

Item	Dimensions and description
Shell-side parameters	
D_o/D_i (mm)	223/211
Material	$0Cr_{18}Ni_9$
Tube parameters	
d_o/d_i (mm)	19/15
Effective length (mm)	1703
Number	37
Layout pattern	45°
Tube pitch (mm)	25
Material	$0Cr_{18}Ni_9$
Baffle parameters	
Baffle pitch (mm)	250
Helix angle	40°
Thickness (mm)	3
Number	24

Energy:

$$\frac{\partial}{\partial x_i}(\rho u_i t) = \frac{\partial}{\partial x_i}\left(\frac{k}{C_P}\frac{\partial t}{\partial x_i}\right) \tag{3}$$

Turbulent kinetic energy:

$$\frac{\partial}{\partial t}(\rho k) + \frac{\partial}{\partial x_i}(\rho k u_i) = \frac{\partial}{\partial x_j}\left(\alpha_k \mu_{eff}\frac{\partial k}{\partial x_j}\right) + G_k + \rho\varepsilon \tag{4}$$

Turbulent energy dissipation:

$$\frac{\partial}{\partial t}(\rho\varepsilon) + \frac{\partial}{\partial x_i}(\rho\varepsilon u_i) = \frac{\partial}{\partial x_j}\left(\alpha_\varepsilon \mu_{eff}\frac{\partial \varepsilon}{\partial x_j}\right) + C^*_{1\varepsilon}\frac{\varepsilon}{k}G_k - C_{2\varepsilon}\rho\frac{\varepsilon^2}{k} \tag{5}$$

where

$$\mu_{eff} = \mu + \mu_t, \quad \mu_t = \rho c_\mu \frac{k^2}{\varepsilon}, \quad C^*_{1\varepsilon} = C_{1\varepsilon} - \frac{\eta(1-\eta/\eta_o)}{1+\beta\eta^3},$$
$$\eta = (2E_{ij}\cdot E_{ij})^{1/2}\frac{k}{\varepsilon}, \quad E_{ij} = \frac{1}{2}\left[\frac{\partial u_i}{\partial x_j} + \frac{\partial u_j}{\partial x_i}\right].$$

The empirical constants for the RNG k–ε model are assigned as following [51]:

$C_\mu = 0.0845$, $C_{1\varepsilon} = 1.42$, $C_{2\varepsilon} = 1.68$, $\beta = 0.012$, $\eta_o = 4.38$, $\alpha_\kappa = \alpha_\varepsilon = 1.39$.

Now boundary conditions are presented. Non-slip boundary condition is applied on the inner wall of the shell and all solid surfaces within the computational domain. The standard wall function method is used to simulate the flow in the near-wall region. The mass-flow-inlet and outflow boundary condition [51] are applied on the inlet and outlet sections, respectively. To the authors' knowledge, such treatments of the inlet and out let conditions are corresponding to the average velocity distribution at the inlet and the fully developed condition [52] at the outlet. The temperature of tube walls are set as constant and their values are taken from the average wall temperature determined in the experiments [18]. The shell wall of heat exchanger is set as adiabatic. Heat conduction of baffles in heat exchanger is considered by using shell conduction in thin-walls model [51] in FLUENT. The baffles are made from stainless steel and its thermal conductivity is taken as constant (15.2 W/(m K)). The conductive-320 oil is taken as working fluid for shell side of heat exchanger in simulation and thermophysical properties of the fluid are listed in Table 2 [18].

2.3. Grid generation and numerical method

The 3D grid system was established using the commercial code GAMBIT based on the 3D geometry created in a commercial CAD program. The computational domain is discretized with unstructured tetrahedral elements and the region adjacent to the tubes is meshed much finer to meet the requirement of wall function method. The meshes of the computational model are shown in Fig. 4. Grid independence tests are carried out to ensure that a nearly grid independent solution can be obtained. In the test, three different grid systems with 9840678, 13553984 and 17759679 cells are adopted for calculation of the whole heat exchanger, and the difference in the overall pressure drop and the average heat transfer coefficient between last two grid systems are around 2%. Thus, considering both the computational time cost and

Table 2
Thermophysical properties of oil.

Parameter	Value
c_p (J/kg K)	2270.1
μ (kg/ms)	0.0095
ρ (kg/m^3)	826.1
λ (W/m K)	0.132

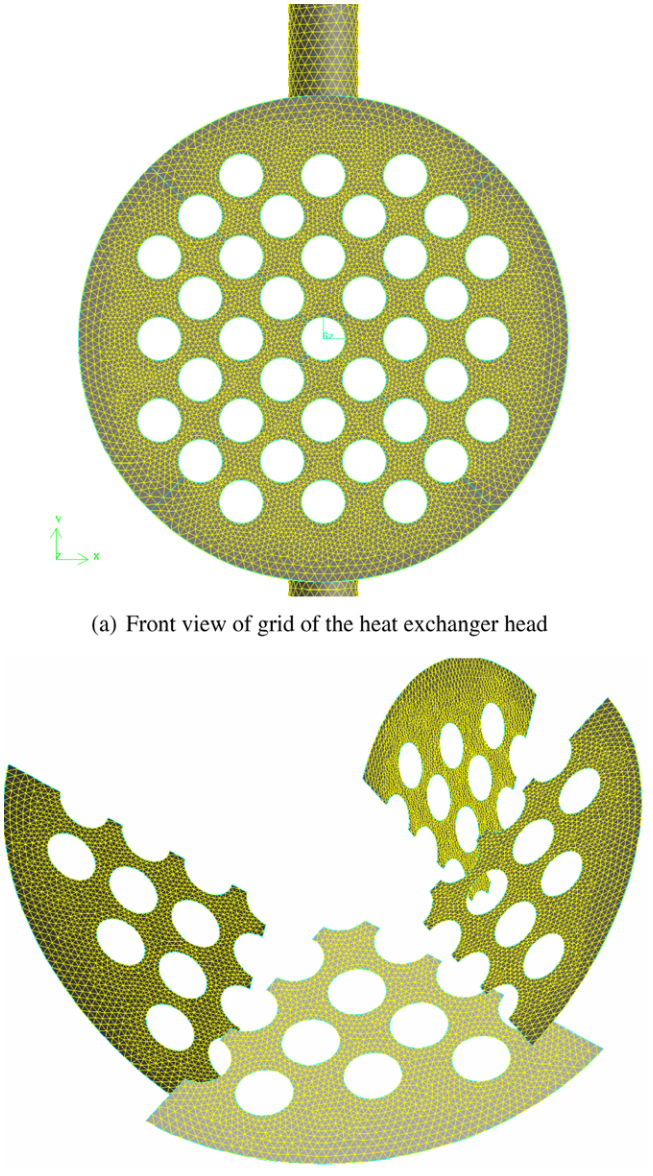

(a) Front view of grid of the heat exchanger head

(b) Details of the baffle grid in one cycle

Fig. 4. Meshes of computational model.

solution precisions the second grid system is taken for the whole computation.

The commercial code FLUENT is adopted to simulate the flow and heat transfer in the computational model. The governing equations are discretized by the finite volume method [52,53]. The QUICK scheme is used to discretize the convective terms. The SIMPLE algorithm is adopted to deal with the coupling between velocity and pressure. The convergence criterion is that the mass residual should be less than 10^{-6} for the flow field and the energy residual less than 10^{-8} for the energy equation. A parallel computation is performed on four DELL workstations with two Quad-Core CPUs and 4 GB memory each by using FLUENT and every simulation case takes approximately 72 h to get converged solutions.

2.4. Data reduction

2.4.1. Determination of shell-side velocity and Re number

The shell-side fluid mean velocity is defined by

$$u = \frac{q_s}{S} \tag{6}$$

where S is the cross-flow area at the shell centerline [2–4,12,54].

For the noncontinuous helical baffles [12]:

$$S = 0.5B\left[D_i - D_1 + \frac{D_1 - d_o}{t_p}(t_p - d_o)\right] \tag{7}$$

where D_i is the inside diameter of shell, D_1 is the diameter of the tube bundle-circumscribed circle, d_o is the tube outside diameter, and t_p is the tube pitch.

For the middle-overlapped helical baffle B is determined as follows:

$$B = \sqrt{2}D_i \cdot \tan\beta \tag{8}$$

With the mean velocity at hand, the Reynolds number of shell-side fluid can be calculated:

$$Re_s = \frac{ud_o}{v_s} \tag{9}$$

It should be emphasized that for the STHXsHB because the shell-side flow pattern resulted from the helical-type structure is close to helical flow, the cross section area is actually only half of the entire cross section at the shell centerline of the heat exchanger.

2.4.2. Shell-side heat transfer coefficient and Nu number

Heat exchange rate of shell-side fluid:

$$\Phi_s = M_s \times c_{ps} \times (t_{s,in} - t_{s,out}) \tag{10}$$

The shell-side heat transfer coefficient h_s is equal to [55]

$$h_s = \frac{\Phi_s}{A_o \cdot \Delta t_m} \tag{11}$$

$$A_o = N_t \cdot \pi d_o l \tag{12}$$

$$\Delta t_m = \frac{\Delta t_{\max} - \Delta t_{\min}}{\ln(\Delta t_{\max}/\Delta t_{\min})} \tag{13}$$

$$\Delta t_{\max} = t_{s,in} - t_w \tag{14}$$

$$\Delta t_{\min} = t_{s,out} - t_w \tag{15}$$

$$Nu_s = \frac{h_s d_o}{\lambda_s} \tag{16}$$

where A_o is the heat exchange area based on the outer diameter of tube; t_w is the temperature of tube walls; the subscripts s and t refer to shell side and tube side, respectively.

3. Computational model validation and result analysis

3.1. Model validation

In order to validate above simulation model simulations are first conducted for the STHXHB described in Table 1. Figs. 5 and 6 provide the comparisons between experimental and numerical results for total shell-side pressure drop and average Nu number, respectively. The experimental data are taken from [18]. It can be observed that for both fluid pressure drop and heat transfer their variation trends with mass flow are in good agreement with the test data. Quantitatively, the maximum differences between numerical results and experimental data are around 25% for pressure drop and 15% for Nu number. It is noticed that the pressure drop of the test data are lower than those of numerical predictions and the Nusselt number of the test data are higher than those of numerical predictions. Apart from some un-avoidable measurement errors, such discrepancies between experimental data and numerical results may be caused by the major simplification made in the computational model: the effect of leakage flow was not ta-

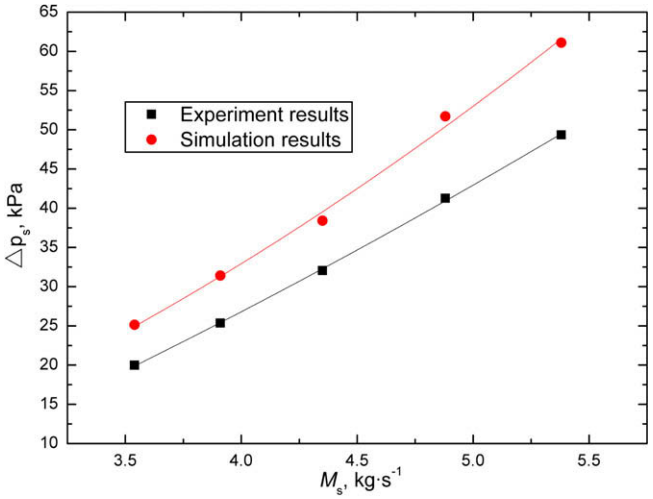

Fig. 5. Comparison of overall pressure drop between experimental results and simulation results in shell side.

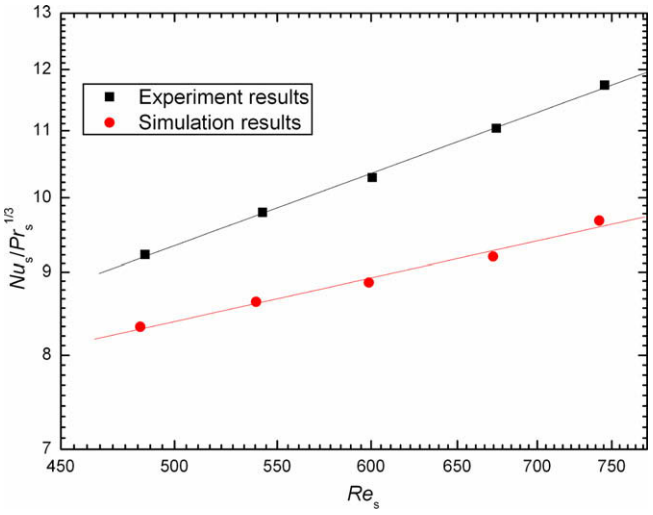

Fig. 6. Comparison of Nu number between experimental results and simulation results in shell side.

ken into account in the simulation. It can be easily understood that this simplification will lead to a higher pressure drop, for the same flow rate the case without leakage and the case with leakage have different actual flow areas. Obviously at the same nominal flow area the one with flow leakage has larger actual flow area than the one without leakage. Thus the pressure drop of the former is expected to be lower than the later. As far as the heat transfer is concerned, the case with leakage also has a larger heat transfer area than the case without leakage for which the only heat transfer surface is the tube-banks. Thus the total heat transfer rate of the case with leakage can be expected larger than that without flow leakage.

The flow path lines in the shell side of the heat exchanger are shown in Fig. 7. It can be clearly observed that except the inlet end region the fluid passes though the tube bundles basically in a helical pattern. By careful examining different flow path lines shown by different colors, it can be observed that in the first four cycles some path lines move forward in a more or less zigzag manner. Only in the fifth and sixth cycles most of the fluid path lines have become quite smooth. This observation may be regarded as an indication of the development process of the periodically fully developed flow of the shell-side, and is quite consistent with the previous measurement results [37–39]. The variation of the cycle average Nusselt number presented later will further support this observation.

3.2. Pressure and temperature variations

In order to observe of the pressure and temperature evolution processes of the shell-side fluid some geometric specifications are made in Fig. 8 to identify each cycle. As can be seen there, the four cycles located in the center part of the heat exchangers are identified as 2–5, respectively. Around the four cycles there are five cross sections which are designated as (a)–(e), respectively. In Fig. 9 the shell-side pressure variations are presented for the above specified geometric units. It should be noted that there are several tube-like space units going through the five cross sections. These are the shell-side fluid space in the central longitudinal section (x–z plane at $y = 0$ and y–z plane at $x = 0$). The hollow tube-like space units are actually the location of tubes. It can be seen that in this visualized space the fluid pressure is the highest at the upper part of cross section (a) and the lowest at the lower part of cross section (e). Totally speaking fluid pressure decreases gradually from cross section (a) to cross section (e). Such variation trend is very understandable.

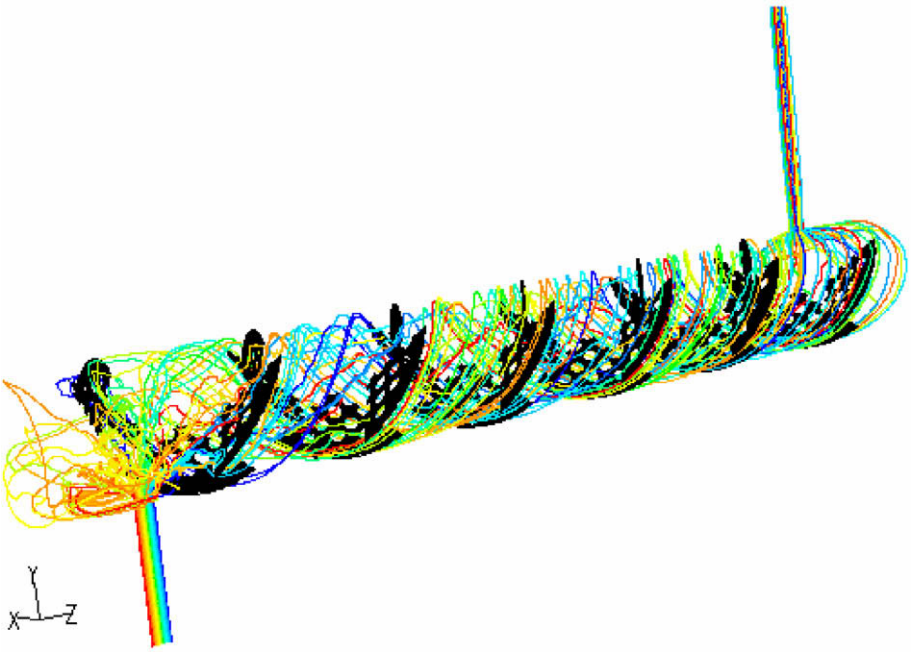

Fig. 7. Path lines in shell side of heat exchanger (M_s = 3.91 kg/s).

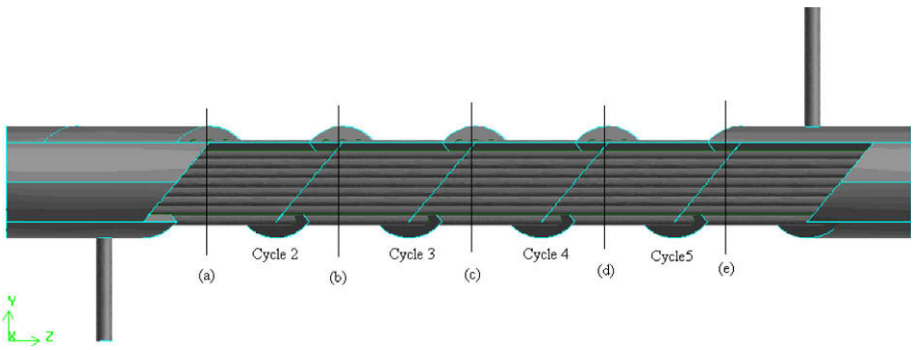

Fig. 8. Specifications of specified surfaces and geometric cycle units.

The variation of shell-side fluid temperature is shown in Fig. 10 with the same visualized method. The streamwise decrease of fluid temperature can be clearly observed. In this computation the tube wall temperature is taken as 289.4 K, and the inlet oil temperature is 318.5 K. It can be seen that in the most part of the helical baffles the solid temperatures are basically dominated by the wall temperature via the conduction. While in the periphery region of each helical baffle, where the tube wall conduction effect is weakened the solid temperatures become higher.

3.3. Variation of the cycle average Nusselt number with cycle

A comparison of pressure drop and *Nu* number between cycles 2 and 5 in whole model (see Fig. 8) at a fixed mass flow rate are presented in Table 3. Two basic features can be observed. First, as in the external flow passing through geometrically periodic structure [37–39], the cycle average Nusselt number is the largest in the inlet cycle of the simulated STHXHB, and then its values gradually deceases in the streamwise direction, even though the variation is not as significant as that in [37–39]. Second as far as the absolute value is concerned, the Nusselt number of the fifth cycle differs from that of the second cycle by less than 2.0 %. And the difference between the fourth cycle and the fifth cycle is even less than 0.5%.

Table 3
Comparison of pressure drop and *Nu* number (M_s = 3.54 kg/s).

Item	Pressure drop (Pa)	*Nu* number
Cycle 2 in whole model	138.01	44.19
Cycle 3 in whole model	130.97	43.71
Cycle 4 in whole model	130.95	43.51
Cycle 5 in whole model	135.58	43.36

The same comparison results can be obtained for the fluid pressure drop. Therefore from fifth cycle the flow and heat transfer in STHXHB can be regarded as periodically fully developed. As an engineering computation, 1–2% discrepancy can be accepted. Thus from the present simulation the periodic model for one cycle can be accepted for the performance simulation of a STHXHB within the accuracy allowed in engineering computation to greatly save the computer source.

4. Conclusion

In this paper, a comprehensive simulation model for a whole STHXHB with middle-overlapped baffles is developed by using

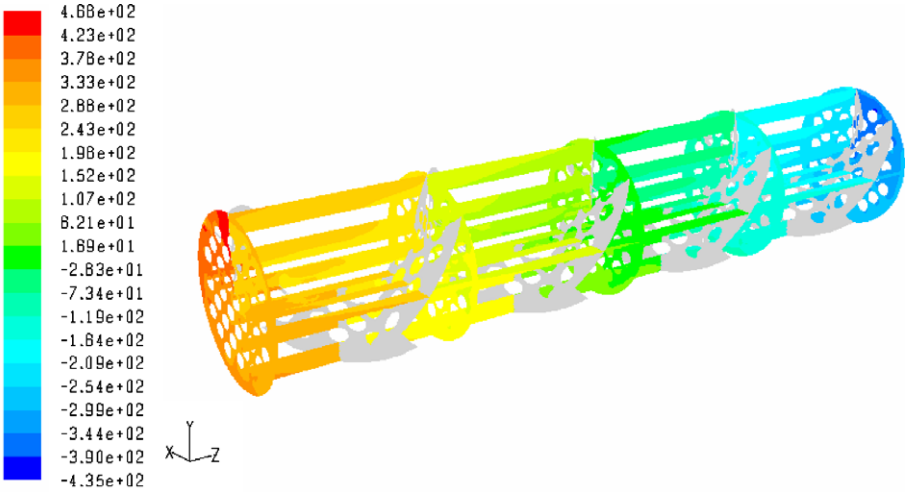

Fig. 9. Pressure distribution in specified surfaces of shell side without inlet and outlet sections (faces (a)–(e) in Fig. 8, *x*–*z* longitudinal section at *y* = 0 and *y*–*z* longitudinal section at *x* = 0, M_s = 3.91 kg/s).

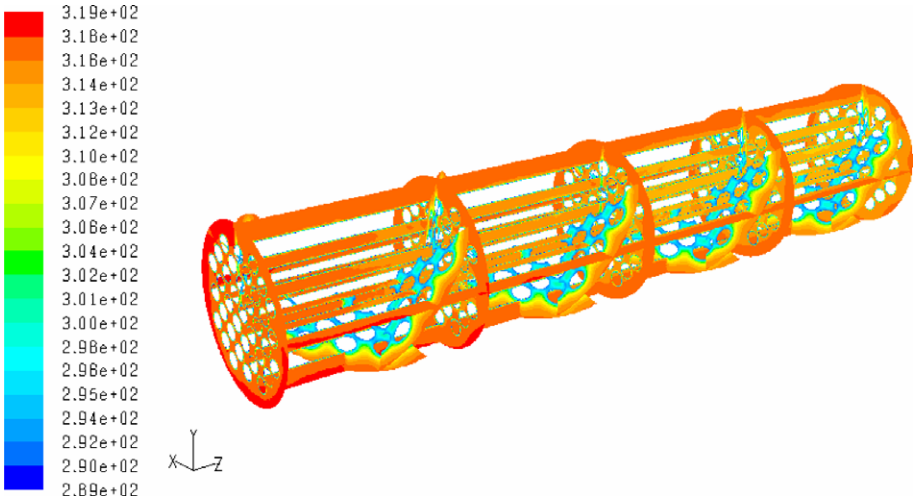

Fig. 10. Temperature distribution in specific surfaces of shell side without inlet and outlet sections (faces (a)–(e) in Fig. 8, *x*–*z* longitudinal section at *y* = 0 and *y*–*z* longitudinal section at *x* = 0, M_s = 3.91 kg/s).

commercial code FLUENT and the grid generation program GAMBIT. Validation for the helical angle of 40° helix angle is performed and the numerical results show a reasonable agreement with the available experiment data.

Simulation of the shell-side fluid flow and heat transfer for the whole heat exchanger is conducted. Comparison between cycle average Nusselt number and the pressure drop shows that the absolute value of the cycle average Nusselt number decreases from the inlet to outlet, so does the pressure drop. However, the relative differences are quite mild and for the case studied the difference between the 2nd cycle and the fifth cycles are both less than 2% for both pressure drop and heat transfer. Thus for the performance simulation of a STHXHB periodic model for one cycle can be used to investigate its performance without inducing large error.

In the companion paper simulations by using periodic models will be conducted and parameter effects will be investigated.

Acknowledgments

This work is supported by the National Fundamental Research Program of China (973 Program) (2007CB206902), the Key Project of Chinese Ministry of Education (No. 306014) and the Key Project of National Natural Science Foundation of China (No. 50636050).

References

[1] B.I. Master, K.S. Chunangad, V. Pushpanathan, Fouling mitigation using helixchanger heat exchangers, in: Proceedings of the ECI Conference on Heat Exchanger Fouling and Cleaning: Fundamentals and Applications, Santa Fe, NM, May 18–22 2003, pp. 317–322.
[2] K.J. Bell, Delaware method for shell side design, in: S. Kakac, A.E. Bergles, F. Mayinger (Eds.), Heat Exchangers-Thermal-Hydraulic Fundamentals and Design, Taylor & Francis, Washington, DC, 1981.
[3] K.J. Bell, Delaware method of shell side design, in: J.W. Pallen (Ed.), Heat Exchanger Sourcebook, Hemisphere, New York, 1986.
[4] K.J. Bell, Delaware method of shell-side design, in: R.K. Shah, E.C. Sunnarao, R.A. Mashelkar (Eds.), Heat Transfer Equipment Design, Taylor & Francis, New York, 1988.
[5] K.J. Bell, Heat exchanger design for the process industries, ASME J. Heat Transfer 126 (6) (2004) 877–885.
[6] R. Mukherjee, Use double-segmental baffles in the shell-and-tube heat exchangers, Chem. Eng. Prog. 88 (1992) 47–52.
[7] M. Saffar-Avval, E. Damangir, A general correlation for determining optimum baffle spacing for all types of shell and tube exchangers, Int. J. Heat Mass Transfer 38 (13) (1995) 2501–2506.
[8] H.D. Li, V. Kottke, Effect of baffle spacing on pressure drop and local heat transfer in shell-and-tube heat exchangers for staggered tube arrangement, Int. J. Heat Mass Transfer 41 (10) (1998) 1303–1311.
[9] P. Sthlik, V.V. Wadekar, Different strategies to improve industrial heat exchange, Heat Transfer Eng. 23 (6) (2002) 36–48.
[10] B.K. Soltan, M. Saffar-Avval, E. Damangir, Minimization of capital and operating costs of shell and tube condensers using optimum baffle spacing, Appl. Thermal Eng. 24 (17–18) (2004) 2801–2810.
[11] J. Lutcha, J. Nemcansky, Performance improvement of tubular heat exchangers by helical baffles, Trans. Inst. Chem. Eng. 68 (1990) 263–270.
[12] P. Stehlik, J. Nemcansky, D. Kral, Comparison of correction factors for shell-and-tube heat exchangers with segmental or helical baffles, Heat Transfer Eng. 15 (1) (1994) 55–65.
[13] D. Kral, P. Stelik, H.J. Van Der Ploeg, Bashir I. Masster, Helical baffles in shell-and-tube heat exchangers, Part One: experimental verification, Heat Transfer Eng. 17 (1) (1996) 93–101.
[14] S.L. Wang, Hydrodynamic studies on heat exchangers with helical baffles, Heat Transfer Eng. 23 (3) (2002) 43–49.
[15] Z.G. Zhang, T. Xu, X.M. Fang, Experimental study on heat transfer enhancement of a helically baffled heat exchanger combined with three-dimensional finned tubes, Appl. Thermal Eng. 24 (14–15) (2004) 2293–2300.
[16] B. Peng, Q.W. Wang, C. Zhang, G.N. Xie, L.Q. Luo, Q.Y. Chen, M. Zeng, An experimental study of shell-and-tube heat exchangers with continuous helical baffles, ASME J. Heat Transfer 129 (2007) 1425–1431.
[17] Yong-Gang Lei, Ya-Ling He, Pan Chu, Rui Li, Design and optimization of heat exchangers with helical baffles, Chem. Eng. Sci. 63 (2008) 4386–4395.
[18] Jian-Fei Zhang, Bin Li, Wen-Jiang Huang, Yong-Gang Lei, Ya-Ling He, Wen-Quan Tao, Experimental performance comparison of shell side heat transfer for shell-and-tube heat exchangers with middle-overlapped helical baffles and segmental baffles, Chem. Eng. Sci. 64 (2009) 1643–1653.
[19] S.V. Patankar, D.B. Spalding, A calculation procedure for the transient and steady state behavior of shell-and-tube heat exchanger, in: N.F. Afgan, E.U. Schlunder (Eds.), Heat Exchanger Design and Theory Source Book, McGraw-Hill, New York, 1974.
[20] D. Butterworth, A model for heat transfer during three-dimensional flow in tube bundles, in: 6th International Heat Transfer Conference, Toronto, August 1978.
[21] W.T. Sha, An overview on rod-bundle thermal-hydraulic analysis, Nucl. Eng. Des. 62 (1980) 1–24.
[22] W.T. Sha, C.I. Yang, T.T. Kao, et al., Multi-dimensional numerical modeling of heat exchangers, ASME J. Heat Transfer 104 (1982) 417–425.
[23] M. Prithiviraj, M.J. Andrews, Three-dimensional numerical simulation of shell-and-tube heat exchanger, Part I: foundation and fluid mechanics, Numer. Heat Transfer A Appl. 33 (1998) 799–816.
[24] M. Prithiviraj, M.J. Andrews, Three-dimensional numerical simulation of shell-and-tube heat exchanger, Part II: heat transfer, Numer. Heat Transfer A Appl. 33 (1998) 817–828.
[25] M. Prithiviraj, M.J. Andrews, Comparison of a three-dimensional numerical model with existing methods for prediction of flow in shell-and-tube heat exchangers, Heat Transfer Eng. 20 (2) (1999) 15–19.
[26] Bin Deng, Experimental and numerical study of flow and heat transfer in the shell side of heat exchangers, Ph.D. dissertation, Xi'an Jiaotong University, Xi'an, China, 2003.
[27] M.J. Andrews, B.I. Master, 3-D modeling of the ABB Lummus Heat Transfer Helixchanger using CFD, in: International Conference Compact Heat Exchangers, Banff, Canada, July 19–23, 1999.
[28] M.J. Andrews, B.I. Master, Three-dimensional modeling of a Helixchanger® heat exchanger using CFD, Heat Transfer Eng. 26 (2005) 22–31.
[29] K. Schröder, H. Gelbe, Two- and three-dimensional CFD-simulation of flow-induced vibration excitation in tube bundles, Chem. Eng. Process. 38 (1999) 621–629.
[30] U. Mohr, H. Gelbe, Velocity distribution and vibration excitation in tube bundle heat exchangers, Int. J. Thermal Sci. 39 (2000) 414–421.
[31] C. Philpott, J. Deans, The enhancement of steam condensation heat transfer in a horizontal shell and tube condenser by addition of ammonia, Int. J. Heat Mass Transfer 47 (2004) 3683–3693.
[32] T. Karlsson, L. Vamling, Flow fields in shell-and-tube condensers: comparison of a pure refrigerant and a binary mixture, Int. J. Refrigeration 28 (2005) 706–713.
[33] S.H. Lee, N. Hur, Numerical analysis of the fluid flow and heat transfer in a shell and tube heat exchanger, in: Proceedings of 1st Asian Symposium on Computational Heat Transfer and Fluid Flow, Xi'an, China, October 18–21 2007.
[34] R.J. Shen, X. Feng, X.D. Gao, Mathematical model and numerical simulation of helical baffles heat exchanger, J. Enhanced Heat Transfer 11 (2004) 461–466.
[35] Yong-Gang Lei, Ya-Ling He, Rui Li, Ya-Fu Gao, Effects of baffle inclination angle on flow and heat transfer of a heat exchanger with helical baffles, Chem. Eng. Process. Process Intensification 47 (12) (2008) 2336–2345.
[36] M.R. Jafari Nasr, A. Shafeghat, Fluid flow analysis and extension of rapid design algorithm for helical baffle heat exchangers, Appl. Thermal Eng. 28 (2008) 1324–1332.
[37] S.S. Lue, H.Z. Huang, W.Q. Tao, Experimental study on heat transfer and pressure drop characteristics in the developing region for arrays of obliquely positioned plates of nonuniform length, Exp. Thermal Fluid Sci. 7 (1993) 30–38.
[38] H.Z. Huang, W.Q. Tao, An experimental study on heat mass transfer and pressure drop characteristics for arrays of nonuniform plate length positioned obliquely to the flow direction, ASME J. Heat Transfer 115 (1993) 568–575.
[39] L.B. Wang, W.Q. Tao, Heat transfer and fluid flow characteristics of plate array aligned at angles to the flow direction, Int. J. Heat Mass Transfer 38 (1995) 3053–3063.
[40] Z.Y. Guo, D.Y. Li, B.X. Wang, A novel concept for convective heat transfer enhancement, Int. J. Heat Mass Transfer 41 (1998) 2221–2225.
[41] S. Wang, Z.X. Li, Z.Y. Guo, Novel concept and device of heat transfer augmentation, in: Proceedings of 11th International Heat Transfer Conference, vol. 5, 1998, pp. 405–408.
[42] Z.Y. Guo, S. Wang, Novel concept and approaches of heat transfer enhancement, in: Cheng P. (Ed.), Proceedings of Symposium on Energy Engineering in the 21th Century, Begell House, vol. 1, New York, 2000, pp. 118–126.
[43] B. Hua, P.S. Guo, S.S. Lu, et al. The study of field synergy theory in transfer process, in: Proceeding of 2001 IAMS International Seminar on Materials for Use in Lithium Battery and Transport Phenomena in Material Processing, Japan, November 2001, pp. 26–27.
[44] W.Q. Tao, Z.Y. Guo, B.X. Wang, Field synergy principle for enhancing convective heat transfer - its extension and numerical verifications, Int. J. Heat Mass Transfer 45 (2002) 3849–3856.
[45] W.Q. Tao, Y.L. He, Q.W. Wang, et al., A unified analysis on enhancing single phase convective heat transfer with field synergy principle, Int. J. Heat Mass Transfer 45 (2002) 4871–4879.
[46] S. Shen, W. Liu, W.Q. Tao, Analysis on field synergy on natural convective heat transfer in porous media, Int. Commun. Heat Mass Transfer 30 (8) (2003) 1081–1090.
[47] Y.P. Cheng, Z.G. Qu, W.Q. Tao, et al., Numerical design of efficient slotted fin surface based on the field synergy principle, Numer. Heat Transfer A Appl. 45 (6) (2004) 517–538.

[48] Y.L. He, M. Wu, W.Q. Tao, et al., Improvement of the thermal performance of pulse tube refrigerator by using a general principle for enhancing energy transport and conversion processes, Appl. Thermal Eng. 24 (2004) 79–93.
[49] Z.Y. Guo, W.Q. Tao, R.K. Shah, The field synergy (coordination) principle and its applications in enhancing single phase convective heat transfer, Int. J. Heat Mass Transfer 48 (2005) 1797–1807.
[50] V. Yakhot, S.A. Orszag, Renormalization group analysis of turbulence 1: basic theory, J. Sci. Comput. 1 (1996) 3–11.
[51] FLUENT 6.3 user's guide, FLUENT Inc., 2006, section 12.4.2, section 7.5, section 7.10, section 7.13.1.
[52] W.Q. Tao, Numerical Heat Transfer, second ed., Xi'an Jiaotong University Press Xi'an, China, 2001.
[53] S.V. Patakar, Numerical Heat Transfer and Fluid Flow, McGraw-Hill Company, New York, 1980.
[54] Ernst U. Schlünder (Ed.), Heat Exchanger Design Handbook, vol. 3, Hemisphere Publishing Corporation, Washington, 1983. p. 3.3.5-16.
[55] S.M. Yang, W.Q. Tao, Heat Transfer, third ed., High Education Press, Beijing, China, 1998. 163–164.